International Journal of Minerals, Metallurgy and Materials
Volume 23, Number 6, June 2016, Page 618
DOI: 10.1007/s12613-016-1274-4

Infiltration behavior of sintering liquid on nuclei ores during low-titanium ore sintering process

Dong-hui Liu, Jian-liang Zhang, Xun Xue, Guang-wei Wang, Ke-jiang Li, and Zheng-jian Liu

School of Metallurgy and Ecological Engineering, University of Science and Technology Beijing, Beijing 100083, China
(Received: 21 October 2015; revised: 24 November 2015; accepted: 30 November 2015)

Abstract: Sinter strength is dependent not only on the self-intensity of the residual rude and bonding phase but also on the bonding degree between them. The infiltration behavior of sintering liquid on nuclei ores influences the bonding degree, which ultimately determines the sinter strength. Infiltration tests were conducted using micro-sinter equipment. The infiltration area index of original liquid (IAO), infiltration volume index of secondary liquid (IVS), and sinter body bonding strength (SBS) were proposed to study the melt infiltration behavior. The results show that the IVS first increases and then decreases with increasing TiO_2 content in adhering fines, whereas the IAO exhibits the opposite behavior. Compared with the original liquid, the secondary liquid shows lower porosity, smaller pores, and more uniform distribution. The SBS increases first and then decreases with increasing IAO and TiO_2 content, and reaches a maximum when the IAO and TiO_2 contents are approximately 0.5 and 2.0wt%, respectively. The SBS first increases and then tends to be stable with increasing IVS. The TiO_2 content is suggested to be controlled to approximately 2.0wt% in low-titanium ore sintering.

Keywords: titanomagnetite; vanadium ore treatment; ore sintering; infiltration

1. Introduction

Vanadium titanomagnetite is not only an important type of iron-bearing mineral but also the main carrier of vanadium and titanium resources. It has been widely used in vanadium and titanium extraction process and blast furnace production. In China, vanadium titanomagnetite is mainly used in the process of sinter production because of the smelting and extraction particularity. Many studies [1–11] on the sintering behavior of vanadium titanomagnetite concentrate have been reported. The results of these studies indicate that vanadium titanomagnetite concentrate mainly serves to the adhering fines and combines with the nuclei ore to form sinter units in granulation; however, it is disadvantageous for mixture granulation because of the fine particle size. In addition, the high content of TiO_2 in vanadium titano-magnetite results in more perovskite and less silicate and calcium ferrite in sinter, which finally leads to the low strength of sinter and adversely affects the smooth operation of the blast furnace (BF). Therefore, further research on the high-temperature behavior of vanadium titanomagnetite in sintering is necessary.

Kasai *et al.* [12–13] used differential thermal analysis (DTA) to study the effects of chemical composition on the sintering behavior of melt. Wu *et al.* [14-19] proposed the new concept of "iron ores sintering basic characteristics" and studied the effects of the high-temperature behavior of iron ores on the quantity and self-intensity of the bonding phase. Okazaki *et al.* [20] studied the penetrating behavior of melt and identified the influencing factors of penetrating depth. However, it is difficult to avoid basicity segregation for the sinter mixture in the industrial sintering process; the basicity of adhering fines in the local area where melt can be formed tends to be very high. The original melt formed by high-basicity adhering fines infiltrates and flows on the surface of nuclei ores; the infiltration reaction then occurs between the original melt and nuclei ores to generate the secondary melt. These melt constitutes the whole sintering liquid, which bonds with the residual rude to form

Corresponding author: Jian-liang Zhang E-mail: zhang.jianliang@hotmail.com

high-strength sinter. Therefore, the property and quantity of sintering liquid affect the bonding degree between the unmelted materials and bonding phase, which finally determine the consolidation strength of sinter. However, studies on the infiltration behavior of sintering liquid on nuclei ores have rarely been reported.

In the present study, the infiltration behavior of sintering liquid on nuclei ores during low-titanium ore sintering process was investigated. The infiltration area index of original liquid (IAO), infiltration volume index of secondary liquid (IVS), and sinter body bonding strength (SBS) were proposed to improve the quality of vanadium–titanium sinter, providing theoretical evidence for the liquid infiltration mechanism of iron ores during the sintering process.

2. Experimental

2.1. Materials and sample preparation

Return fines, pure CaO, and five kinds of iron ores (named as Ore-A, Ore-B, Ore-C, Ore-D, and Ore-E, respectively) were used in the present study. The chemical composition of iron-bearing materials is listed in Table 1. Ore-A was typical Brazilian hematite with the highest iron content among six iron-bearing materials investigated in this work. Return fines was from BF sieving exhibited the lowest iron content and the highest CaO and SiO_2 content among the iron-bearing materials. Ore-B and Ore-C were typical Australian limonite, whereas Ore-D was normal iron concentrate from China. Ore-E was vanadium titanomagnetite concentrate, which should be used in conjunction with other iron ores because of its poor sintering characteristics.

Table 1. Chemical composition of iron-bearing materials

wt%

Material	TFe	TiO_2	CaO	SiO_2	Al_2O_3	MgO	FeO
Ore-A	66.98	0.13	0.14	2.91	1.51	0.20	0.49
Ore-B	62.04	0.14	0.14	3.93	2.60	0.14	0.34
Ore-C	57.80	0.28	0.69	5.40	2.83	0.50	0.38
Ore-D	61.90	0.23	0.69	6.29	1.36	3.72	23.50
Ore-E	65.02	3.19	0.63	5.00	2.37	0.85	29.18
Return fines	55.00	1.63	10.92	10.92	1.99	2.40	8.64

2.2. Apparatus and methods

To clarify the infiltration behavior of sintering liquid on nuclei ores during the low-titanium ore sintering process, infiltration tests were carried out using micro-sinter equipment. The selected experimental materials were dried at 105°C for 3 h and ground to a size less than 147 μm. Because the mass fractions of adhering fines and nuclei ores in mixed ores were approximately 40wt% and 60wt%, respectively, during industrial sintering process, the calculated binary basicity of adhering fines was approximately 4.0 when the binary basicity of sinter was 2.0. The binary basicity of the fine mixture mixed with iron ore and pure CaO was set to be 4.0 in these experiments; the fine mixture was pressed to the cylinder with a height of 5 mm and a diameter of 8 mm at 15 MPa for 2 min to simulate adhering fines in the sintering process. The return fines was pressed to the cylinder with a height of 7.5 mm and a diameter of 20 mm at 20 MPa for 2 min to simulate nuclei ores coated by adhering fines [14–19]. The cylinder of adhering fines was placed over the cylinder of return fines and sintered in the micro-sinter equipment. The tests were conducted twice for each scheme. The experimental atmosphere used in the first step (0–4 min) was air, that in the second step (4–11.5 min) was N_2, and that in the last step (11.5–25 min) was air; the gas flow during the whole experiment was kept at 3 L/min. The experimental atmosphere and heating curve are shown in Fig. 1.

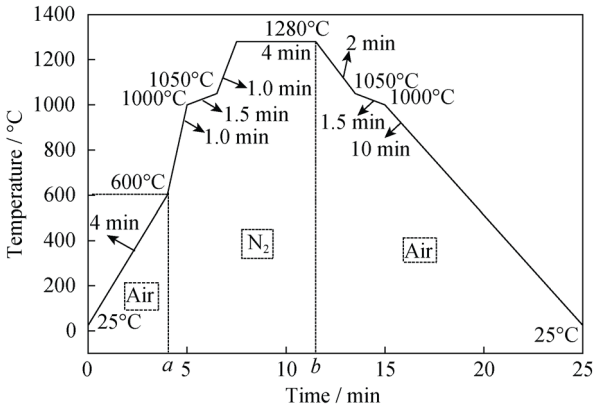

Fig. 1. Graphical presentation of the experimental atmosphere and heating curve.

When the sintered samples were cooled to room temperature, the vertical projection area of the melt formed by adhering fines on the cylinder of return fines was measured using an image analytical method. The first sintered sample was mounted in epoxy resin and dissected perpendicular to the interface in the center; seven groups of liquid infiltration depths of melt on the cylinder of return fines were measured from rim to center, and their average value was calculated. The second sintered sample was placed on the platform of pressure-testing device, and its compressive strength was measure; the sinter body bonding strength (SBS) was expressed as the compressive strength of the sintered sample. The low melting-point liquid formed by the assimilation reaction between iron ores and CaO in adhering fine layers during the sintering process was defined as the original liq-

uid. The melt formed by the infiltration action between original liquid and nuclei ore was defined as the secondary liquid. Fig. 2 shows a schematic of the infiltration tests. To clarify the infiltration behavior of melt on nuclei ores, the infiltration area index of the original liquid (IAO) and the infiltration volume index of the secondary liquid (IVS) were proposed and used to assess the infiltration and bonding ability of iron ores during the sintering process. The calculation formulas of these indexes are shown in Eqs. (1) and (2).

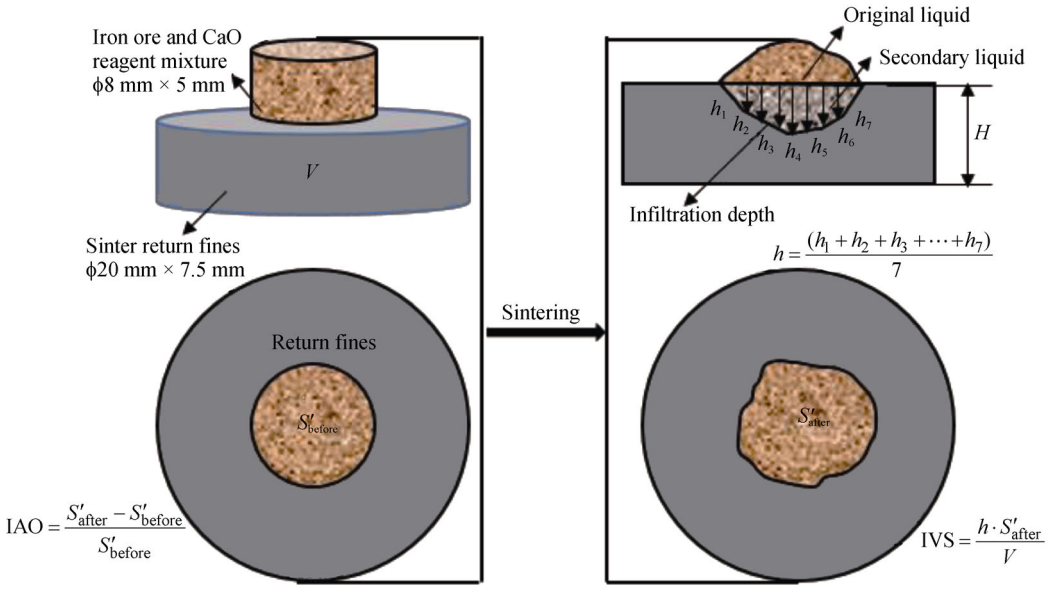

Fig. 2. Schematic of the infiltration test.

$$IAO = \frac{S'_{after} - S'_{before}}{S'_{before}} \quad (1)$$

$$IVS = \frac{h \cdot S'_{after}}{V} \quad (2)$$

where S'_{before} is the vertical projection area of adhering fines cylinder before test, mm^2; S'_{after} the vertical projection area of original liquid flowed on the cylinder of return fines after test, mm^2; h the average value of the infiltration depth of secondary liquid, mm; and V the volume of return fines cylinder, mm^3.

To study the infiltration behavior of melt on nuclei ore during the low-titanium ore sintering process, the schemes of ore proportioning tests were made according to the present scheme of T0.5; the influence of the TiO_2 content in adhering fines on melt infiltration behavior was researched by adjusting the TiO_2 content in the mixed ores in increments of 0.5wt%. The schemes of ore proportioning tests are listed in Table 2.

3. Results and discussion

The infiltration of sintering liquid on nuclei ores mainly included two steps. Firstly, the original liquid formed by high-basicity adhering fines infiltrated and flowed on the surface of nuclei ores, resulting in the adjacent nuclei ores being bonded together with melt diffusion. In sequence, infiltration reaction occurred between the original liquid of high basicity and nuclei ores, then the secondary liquid of low basicity was formed at the same time. Nuclei ores were further penetrated and bonded by melt to achieve the effective bonding in unit range. Therefore, the sinter strength was ultimately determined by the bonding of the original liquid among the adjacent nuclei ores and the bonding of the secondary liquid on nuclei ore in unit range. The calculated chemical composition of mixed ores and liquid infiltration indexes are listed in Table 3.

Table 2. Schemes of ore proportioning tests wt%

Scheme	TiO_2 content	Ore-A	Ore-B	Ore-C	Ore-D	Ore-E
T0.5	0.5	28.36	1.63	49.82	11.33	8.86
T1.0	1.0	23.08	1.33	40.56	9.23	25.80
T1.5	1.5	17.82	1.02	31.30	7.12	42.74
T2.0	2.0	12.55	0.72	22.04	5.01	59.68
T2.5	2.5	7.28	0.42	12.78	2.91	76.62
T3.0	3.0	2.00	0.12	3.52	0.80	93.56

3.1. Influence of TiO_2 content on the infiltration behavior of the original liquid

Fig. 3 shows the relation between the IAO and TiO_2 con-

tent in adhering fines. Original liquid was formed by assimilation reaction between iron ores and CaO in the adhering fine layers. The IAO represented the infiltration and flow ability of the original melt on the surface of nuclei ores, which reflected the effective bonding range of melt among adjacent nuclei ores. The results indicate that the IAO decreases with increasing TiO_2 content and reaches a minimum of 0.1470 when TiO_2 content is approximately 1.7wt%, after the IAO starts to increase. The IAO ranges from 0.1470 to 1.0235. The infiltration and flow of the original liquid are blocked to a certain extent due to the coarse surface of nuclei ores, so the values of IAO are relatively high.

Table 3. Calculated chemical composition of mixed ores and liquid infiltration indexes

Scheme	Chemical composition / wt%						IAO	*h* / mm	IVS	SBS / N
	TiO_2	TFe	SiO_2	CaO	MgO	Al_2O_3				
T0.5	0.50	65.02	5.00	0.55	0.85	2.37	1.0235	1.465	0.0633	2800
T1.0	1.00	65.02	5.00	0.56	0.85	2.37	0.3410	2.315	0.0662	3098
T1.5	1.50	65.02	5.00	0.58	0.85	2.37	0.1470	2.940	0.0720	3031
T2.0	2.00	65.02	5.00	0.59	0.85	2.37	0.4161	2.895	0.0875	3215
T2.5	2.50	65.02	5.00	0.61	0.85	2.37	0.7069	2.364	0.0824	3195
T3.0	3.00	65.02	5.00	0.62	0.85	2.37	0.8496	1.887	0.0745	3090

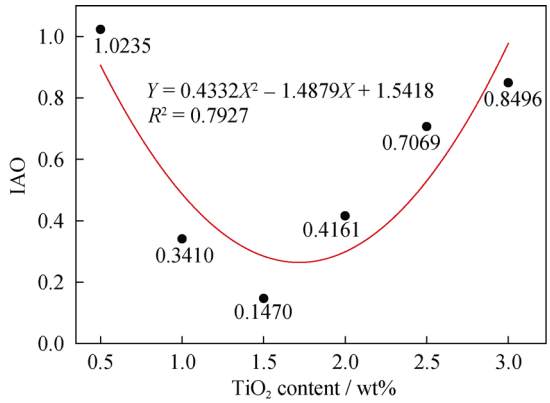

Fig. 3. Relation between IAO and TiO_2 content in adhering fines.

Fig. 4 shows the mineralogical morphology of the original liquid at different TiO_2 content. Many large, well-rounded pores are distributed irregularly in the whole original liquid; the pores become larger in sinter structure with increasing TiO_2 content. The minerals mainly include calcium ferrite, hematite, magnetite, and calcium silicate, among which calcium ferrite is the main bonding phase.

Because the basicity of adhering fines was set to be 4.0, a large amount of low melting-point liquid, for example, calcium ferrite, was generated in the sintering atmosphere. The presence of such low-melting liquids was beneficial to heat and mass transfer during the sintering process [21], and the infiltration and flow of melt on the surface of nuclei ores were promoted. However, the large flow range and poor temperature control of melt resulted in the thin bonding layer among nuclei ore particles. In addition, since the short time and fast rate of sinter reaction, the gases generated from the decomposition reaction of crystal water and carbonate remained in melt and did not have sufficient time to spread. The mineralogical morphology of the original liquid presented the structure of thin-wall and big holes as well as high porosity.

The reactions between TiO_2, Fe_2O_3, and CaO in the sintering process are represented as following equations.

$$CaO + TiO_2 = CaO{\cdot}TiO_2,$$

$$\Delta G^{\ominus} = -19100 - 0.8T, \text{ J/mol} \quad (3)$$

$$CaO + Fe_2O_3 = CaO{\cdot}Fe_2O_3,$$

$$\Delta G^{\ominus} = -1700 - 1.15T, \text{ J/mol} \quad (4)$$

Eqs. (3) and (4) show that the reaction between TiO_2 and CaO is thermodynamically favored over that between Fe_2O_3 and CaO at the same temperature. The reactant concentration in Eq.(3) increased with increasing TiO_2 content, which was beneficial to the forward reaction to form perovskite and simultaneously inhibit the formation of calcium ferrite. The high melting-point perovskite was irregularly dispersed in the melt, which impeded the flow of melt on the surface of nuclei ores; therefore, the IAO decreased and sintering melt distributed unevenly in the sintering bed, leading to an increase in the number of holes and the larger pores being distributed in the mineral phase when the sinter cooled. However, the ratio of vanadium titanomagnetite (Ore-E) increased with increasing TiO_2 content in the adhering fines. As evident in the binary phase diagram of CaO–Fe_2O_3 [22–23], the superheat of the melt formed by vanadium titanomagnetite was relatively higher than that of the melt formed by other iron ores at the same temperature, leading to the low viscosity and strong fluidity of the original liquid. Therefore, the IAO first decreased and then increased with increasing TiO_2 content.

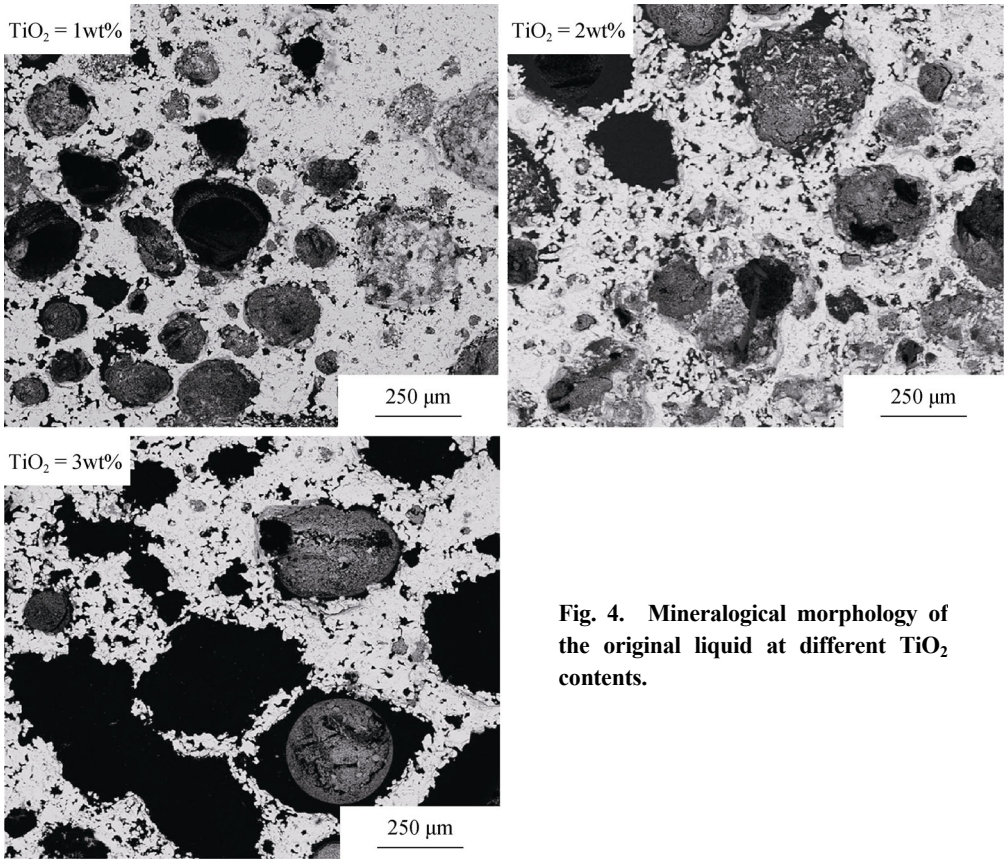

Fig. 4. Mineralogical morphology of the original liquid at different TiO_2 contents.

3.2. Influence of TiO_2 content on the infiltration behavior of the secondary liquid

Nuclei ores were infiltrated and bonded by the secondary liquid to achieve the effective bonding between nuclei ore and melt in unit range. The infiltration behavior of melt influenced the quantity and properties of both original liquid and secondary liquid. The more drastic the infiltration reaction was between melt and nuclei ores, the more the secondary liquid and the less the original liquid would be [24]. With increasing infiltration degree, the fluidity and bonding range of the original liquid decreased as well as the skeleton role of the nuclei ores; however, the effective bonding volume between nuclei ore and melt in unit range increased and the composition of the melt became more uniform.

Liquid infiltration depth and IVS represented the penetration ability and bonding ability of the secondary liquid on nuclei ores, respectively. Fig. 5 shows the relation between

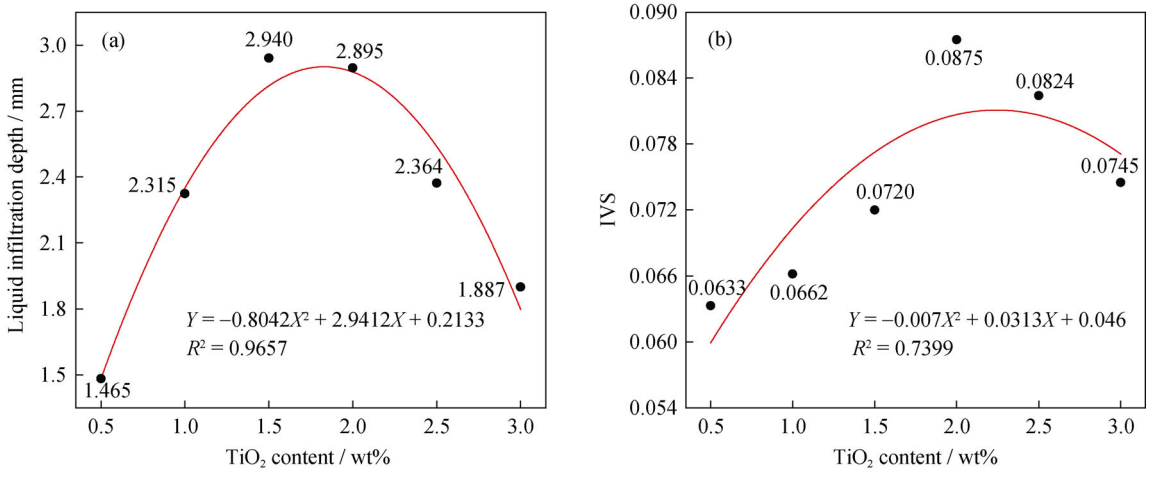

Fig. 5. Relation between TiO_2 content in adhering fines and the infiltration indexes of the secondary liquid: (a) liquid infiltration depth and TiO_2 content; (b) IVS and TiO_2 content.

the TiO_2 content and the infiltration indexes of secondary liquid. It indicates that *h* and IVS first increase and then decrease with increasing TiO_2 content, and IVS is more sensitive to the change of TiO_2 content. Fig. 6 shows the mineralogical morphology of the secondary liquid at various TiO_2 contents. As evident in the figure, the porosity increases, the pores are smaller, and their distribution is more uniform in the secondary liquid compared to the original liquid. Calcium ferrite is also the main bonding phase, whereas the calcium ferrite content decreases somewhat, the hematite and perovskite contents increase. The consolidation of the bonding phase is dominated by the crystal stocks of calcium ferrites, hematite, and silicate slag phases. The porosity increases, the pores become larger, the perovskite content increases, and the calcium ferrite content decreases with increasing TiO_2 content in the sinter structure.

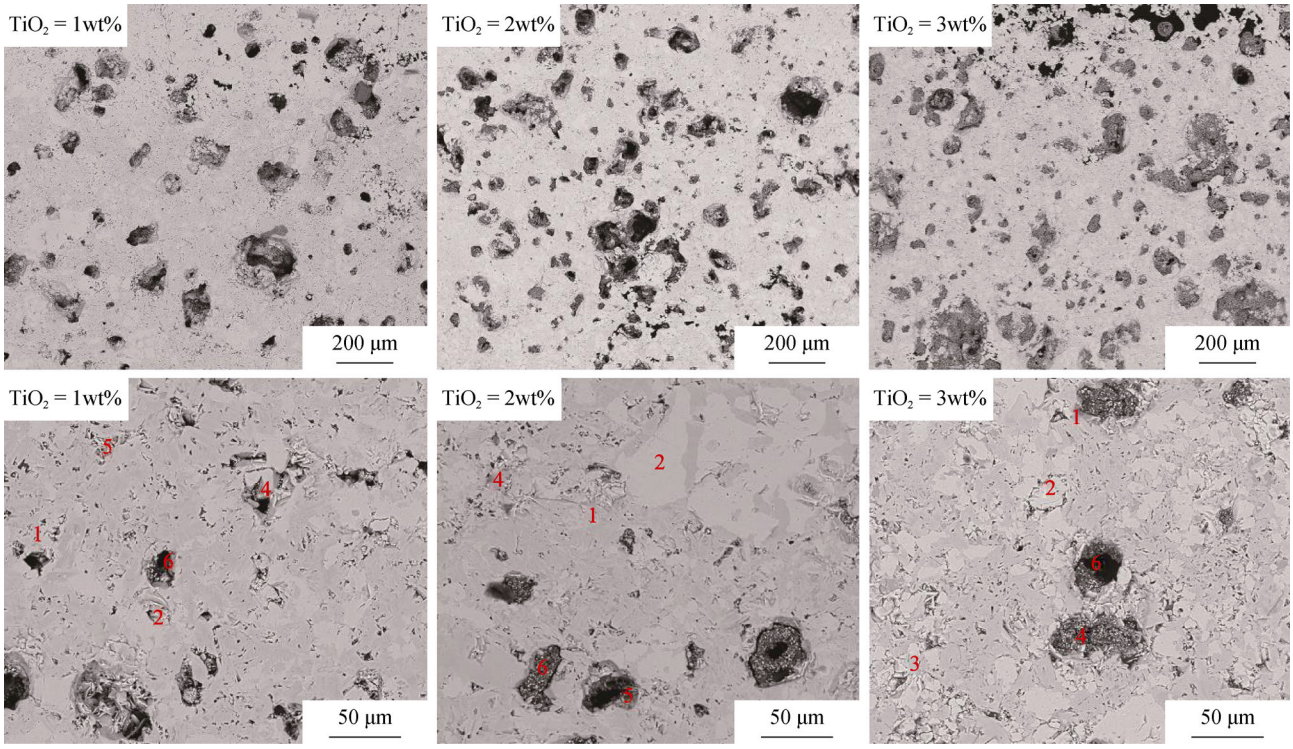

1 — SFCA; 2 — hematite, Fe_2O_3; 3 — perovskite, $CaTiO_3$; 4 — silicate; 5 — magnetite, Fe_3O_4; 6 — pore

Fig. 6. Mineralogical morphology of the secondary liquid at different TiO_2 contents.

The penetration of melt on nuclei ores filled the surrounding pores and achieved the bonding in nuclei ores. The pores in the original liquid shrank during cooling and transferred to the secondary liquid, leading to a smaller size and more uniform distribution of pores in the secondary liquid. The porosity increased and the pores became larger with increasing TiO_2 content, which resulted in an increase in the contact area between the original liquid and nuclei ores. Because the kinetic conditions of the infiltration and penetration reaction were improved, the heat and mass transfer during the sintering process were accelerated. As a result, the infiltration and bonding between the melt and nuclei ores were promoted. However, with continuous increasing TiO_2 content, the melted calcium ferrite and solid ilmennite could react to form perovskite [25]; the corresponding reaction between $CaO{\cdot}Fe_2O_3$ and $FeO{\cdot}TiO_2$ is represented as

$$CaO{\cdot}Fe_2O_3 + FeO{\cdot}TiO_2 = CaO{\cdot}TiO_2 + FeO + Fe_2O_3,$$

$$\Delta G^{\ominus} = -17400 + 0.3T, \text{ J/mol}. \quad (5)$$

Perovskite in the melt filled in the particles of calcium ferrite, hematite, and silicate, leading to the decrease of contact area between the sintering liquid and nuclei ores. As a consequence, the infiltration and bonding between the melt and nuclei ores were limited and the IVS and *h* first increased and then decreased with increasing TiO_2 content.

3.3. Influence of the infiltration behavior of melt on SBS

In the sintering process, unmelted materials were bonded by bonding phases together to form a high-strength sinter body. When the self-intensity of unmelted materials and bonding phases were the same, the bonding degree determined the sinter strength to a large extent. SBS represented the effective bonding strength between the melt and nuclei ores. Fig. 7 shows the influence of sintering liquid infiltra-

tion indexes and TiO_2 content on SBS. It indicates that SBS first increases and then decreases with increasing IAO, *h*, and TiO_2 content. SBS reaches a maximum when IAO, *h*, and the TiO_2 content are 0.5, 2.5 mm, and 2wt%, respectively. SBS first increases and then tends to be stable with increasing IVS.

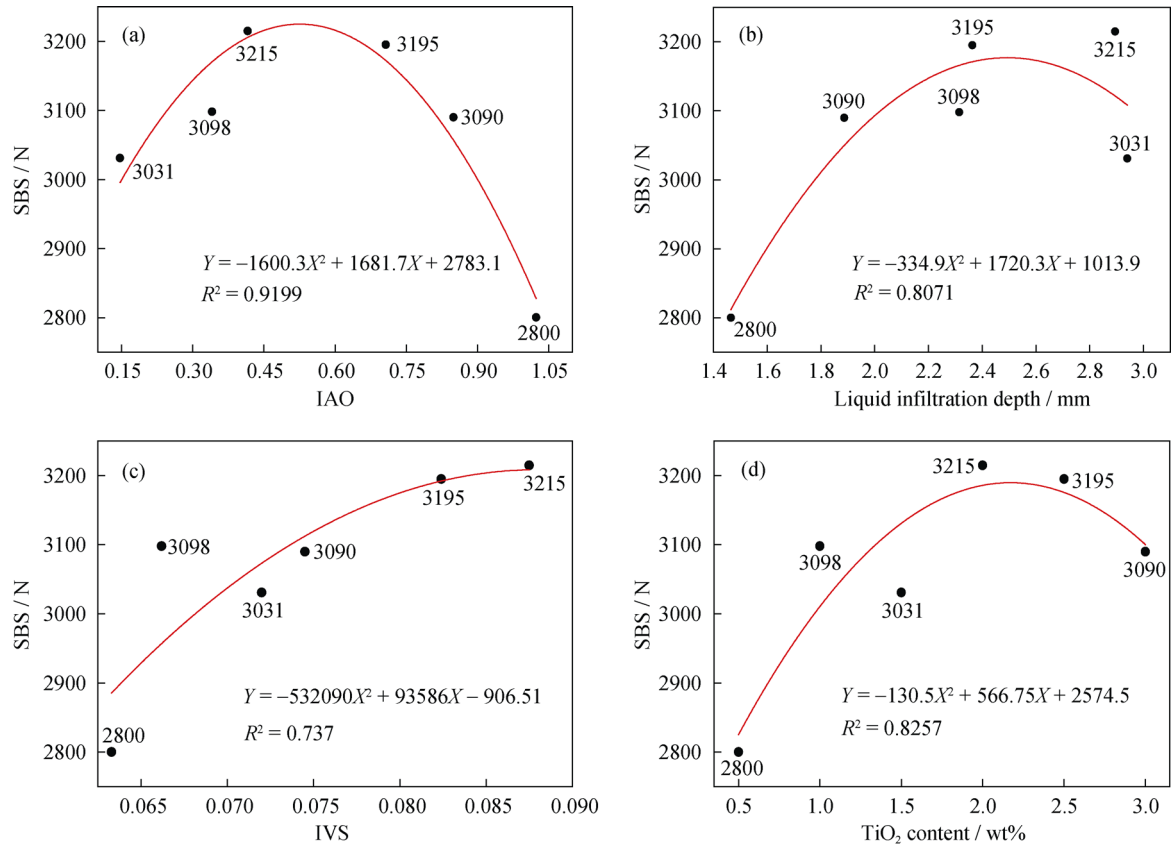

Fig. 7. Influence of sintering liquid infiltration indexes and TiO_2 content on SBS: (a) IAO; (b) *h*; (c) IVS; (d) TiO_2 content.

The increase of IAO meant that the infiltration and flow capability of the original liquid on the surface of nuclei ores were improved; as a result, the contact area between the melt and nuclei ores was augmented, leading to an increase of the effective bonding range and the capability of sintering liquid among adjacent nuclei ores. However, with continuous increasing IAO, the flow range of the melt became larger and the temperature control tended to be poor, leading to a thin bonding layer of the melt among nuclei ore particles. Consequently, adjacent nuclei ores could not be bonded effectively, resulting in a decrease of the SBS.

The increase of *h* meant that the composition of melt was more uniform and that the bonding stability between the nuclei ores and melt was enhanced, which promoted the effective bonding between the sintering liquid and nuclei ores in a unit range. However, with continuous increasing of *h*, because the skeleton role of nuclei ores decreased as well as the melt on the surface of nuclei ores, the effective bonding range of the melt among adjacent nuclei ores decreased, resulting in a decrease of SBS.

The increase of IVS meant that the bonding amount of melt on nuclei ores in a unit range increased; consequently, the sintering resistance increased but the vertical sintering velocity decreased, leading to the prolonging of holding time at high temperature and resulting in the full crystallization of minerals and the densification of sinter structure. However, because unmelted materials in the sintering bed did not have sufficient time to melt as IVS increased further, the melt flowability decreased and the bed permeability was deteriorated, all of which adversely affected the sinter strength.

When the behavior of the sintering liquid was the same, SBS would be improved with the increasing self-intensity of the bonding phase. Because the ratio of vanadium titanomagnetite increased with continuous increasing TiO_2 content, Fe^{2+} in the sinter body increased in sintering atmosphere which could improve the bonding phase self-intensity to a certain extent. Because pores in the melt became larger with continuous increasing TiO_2 content, low-strength perovskite increased but high-strength calcium

ferrite decreased; consequently, SBS first increased and then decreased with increasing TiO_2 content.

4. Conclusions

To clarify the infiltration behavior of the sintering liquid on nuclei ores during the low-titanium ore sintering process, IAO, IVS, and SBS were proposed, and the infiltration tests of the melt on nuclei ores were conducted. The influence of TiO_2 content on IAO, IVS, and SBS and the relation between SBS and the liquid infiltration indexes were analyzed.

(1) The basic characteristics of iron ores are further improved by the introduction of IAO, IVS, and SBS, and the high-temperature behaviors and melt effects during the sintering process are more factually reflected. Investigation on the infiltration behavior of the sintering liquid on nuclei ores enables enrichment of the sinter consolidation mechanism and provides a theoretical basis for sinter optimization of ore-proportioning.

(2) IVS first increases and then decreases with increasing TiO_2 content, whereas IAO exhibits the opposite behavior. High TiO_2 content also results in high porosity, large pores, a greater perovskite content, and a lower calcium ferrite content in the sinter. Compared with the original liquid, the secondary liquid shows a lower porosity, smaller pores, and a more uniform distribution. Since the behavior of the melt varies greatly for different iron ores, IAO, IVS, and SBS can be used to evaluate the comprehensive sintering properties of iron-bearing materials.

(3) SBS increases first and then decreases with increasing IAO, h, and TiO_2 content; SBS reaches a maximum when IAO and the TiO_2 content are 0.5 and 2wt%, respectively. SBS increases first and then tends to be stable with increasing IVS. The TiO_2 content is suggested to be controlled at approximately 2.0wt% in the low-titanium ore sintering process.

Acknowledgements

This work was financially supported by the Major State Basic Research Development Program of China (No. 2012CB720401), the Natural Science Foundation of China and Baosteel (No. 51134008), and the National Natural Science Foundation of China (No. U1260202).

References

[1] Z.W. Yu, G.H. Li, T. Jiang, Y.B. Zhang, F. Zhou, and Z.W. Peng, Effect of basicity on titanomagnetite concentrate sintering, *ISIJ Int.*, 55(2015), No. 4, p. 907.

[2] C.E. Loo and B.G. Ellis, Changing bed bulk density and other process conditions during iron ore sintering, *ISIJ Int.*, 54(2014), No. 1, p. 19.

[3] X.W. Lv, Z.G. Lun, J.Q. Yin, and C.G. Bai, Carbothermic reduction of vanadium titanomagnetite by microwave irradiation and smelting behavior, *ISIJ Int.*, 53(2013), No. 7, p. 1115.

[4] X.H. Fan, Z.Y. Yu, M. Gan, X.L. Chen, T. Jiang, and H.L. Wen, Appropriate technology parameters of iron ore sintering process with flue gas recirculation, *ISIJ Int.*, 54(2014), No. 11, p. 2541.

[5] M. Zhou, T. Jiang, S.T. Yang, and X.X. Xue, Sintering behaviors and consolidation mechanism of high-chromium vanadium and titanium magnetite fines, *Int. J. Miner. Metall. Mater.*, 22(2015), No. 9, p. 917.

[6] S.Y. Chen and M.S. Chu, Metalizing reduction and magnetic separation of vanadium titano-magnetite based on hot briquetting, *Int. J. Miner. Metall. Mater.*, 21(2014), No. 3, p. 225.

[7] A. Dehghan-manshadi, J. Manuel, S. Hapugoda, and N. Ware, Sintering characteristics of titanium containing iron ores, *ISIJ Int.*, 54(2014), No. 10, p. 2189.

[8] S. Ren, J.L. Zhang, L.S. Wu, B.X. Su, X.D. Xing, and G.Y. Zhu, Effect of TiO_2 on equilibrium phase sinter at oxygen partial pressure of 5×10^{-3} atm, *Ironmaking Steelmaking*, 41(2014), No. 2, p. 132.

[9] H.P. Pimenta and V. Seshadri, Influence of Al_2O_3 and TiO_2 degradation behaviour of sinter and hematite at low temperatures on reduction, *Ironmaking Steelmaking*, 29(2002), No. 3, p. 175.

[10] E. Park and O. Ostrovski, Reduction of titania-ferrous ore by hydrogen, *ISIJ Int*., 44(2004), No. 6, p. 999.

[11] N.J. Bristow and C.E. Loo, Sintering properties of iron ore mixes containing titanium, *ISIJ Int.*, 32(1992), No. 7, p. 819.

[12] E. Kasai and F. Saito, Note differential thermal analysis of assimilation and melt-formation phenomena in the sintering process of iron ores, *ISIJ Int*., 36(1996), No. 8, p. 1109.

[13] E. Kasai, Y. Sakano, T. Kawaguchi, and Y. Nakamura, Influence of properties of fluxing materials on the flow of melt formed in the sintering process, *ISIJ Int*., 40(2000), No. 9, p. 857.

[14] S.L. Wu, Y. Liu, J.X. Du, K. Mi, and H. Lin, New concept of iron ores sintering basic characteristics, *J. Univ. Sci. Technol. Beijing*, 24(2002), No. 3, p. 254.

[15] S.L. Wu, Y.M. Dai, O. Dauter, Y.D. Pei, J. Xu, and H.L. Han, Optimization of ore blending during sintering based on complementation of high temperature properties, *J. Univ. Sci. Technol. Beijing*, 32(2010), No. 6, p. 719.

[16] J. Zhu, S.L. Wu, J.X. Fan, G.L. Zhang, and Z.G. Que, Effect of the separation of large limonite ore particles in the granulation process of sinter raw materials, *ISIJ Int*., 53(2013), No. 9, p. 1529.

[17] S.L. Wu, J. Zhu, J.X. Fan, G.L. Zhang, and S.G. Chen, Sintering behavior of return fines and their effective utilization

method, *ISIJ Int*., 53(2013), No. 9, p. 1561.
[18] S.L. Wu, G.L. Zhang, S.G. Chen, and B. Su, Influencing factors and effects of assimilation characteristic of iron ores in sintering process, *ISIJ Int*., 54(2014), No. 3, p. 582.
[19] G.L. Zhang, S.L. Wu, S.G. Chen, J. Zhu, J.X. Fan, and B. Su, Optimization of dolomite usage in iron ore sintering process, *ISIJ Int*., 53(2013), No. 9, p. 1515.
[20] J. Okazaki, K. Higuchi, Y. Hosotani, and K. Shinagawa, Influence of iron ore characteristics on penetrating behavior of melt into ore layer, *ISIJ Int*., 43(2003), No. 9, p. 1384.
[21] N.A.S. Webster, M.I. Pownceby, I.C. Madsen, and J.A. Kimpton, Effect of oxygen partial pressure on the formation mechanisms of complex Ca-rich ferrites, *ISIJ Int*., 53(2013), No. 5, p. 774.
[22] B. Phillips and A. Muan, Phase equilibria in the system CaO iron oxide SiO_2 in air, *J. Am. Ceram. Soc.*, 42(1959), No. 9, p. 413.
[23] L. Li, J. Liu, X.R. Wu, X. Ren, W.B. Bing, and L.S. Wu, Influence of Al_2O_3 on equilibrium sinter phase in N_2 atmosphere, *ISIJ Int*., 50(2010), No. 2, p. 327.
[24] S.L. Wu and G.L. Zhang, Liquid absorbability of iron ores and large limonite particle divided adding technology in the sintering process, *Steel Res. Int*., 86(2015), No. 9, p. 1014.
[25] D. Debrincat, C.E. Loo, and M.F. Hutchens, Effect of iron ore particle assimilation on sinter structure, *ISIJ Int*., 44(2004), No. 8, p. 1308.